Electronic Supplementary Material (ESI) for CrystEngComm.

Supporting Information

Cation exchange in an anionic Metal-organic Framework enhancing propylene/propane separation

Xue Zhang, † Hui-Juan Tang, † Min Zeng, Rong Yang, Yu Wang * and Kai-Jie Chen *

[a] Key Laboratory of Special Functional and Smart Polymer Materials of Ministry of Industry and Information Technology, Xi'an Key Laboratory of Functional Organic Porous Materials, School of Chemistry and Chemical Engineering, Northwestern Polytechnical University, Xi'an, Shaanxi, China

∗ Corresponding author. E-mail addresses: wychem@nwpu.edu.cn (Y. Wang) and ckjiscon@nwpu.edu.cn (K. -J. Chen)

†These authors contributed equally to this work.

Table of contents

S4 Supplementary tables

References

S1 General description of 1

According to reported literature, **1** crystallizes in the orthorhombic space group F*ddd* and has a 3D anionic framework built with triangle clusters [Cu_3(μ_3-OH)] and 4-pyrazolecarboxylate, showing ultramicroporous channels with aperture size of 6.3 × 6.8 Å (**Fig. S1**). Because of the negative charge of the framework ([Cu_3(μ_3-OH)(pyc)$_3$]$^-$), an extra free dimethylamine cation is needed to counterbalance, yielding a formula of [Me_2NH_2][Cu_3(μ_3-OH)(pyc)$_3$] for **1**. Previous studies showed that the free $Me_2NH_2^+$ ions can be exchanged by Li^+ ions to improve the pore volume and H_2 uptake.

S2 Supplementary methods

1 Ideal Adsorbed Solution Theory Calculations

1.1 Single-site Langmuir-Freundlich (L-F) model

The selectivity was calculated to evaluate the C_3H_6/C_3H_8 and C_2H_4/C_2H_6 separation performance based on the IAST method. Single-site Langmuir-Freundlich model was used to fit the C_3H_8 or C_3H_6 adsorption isotherms obtained at 273 K and 298 K.

$$q = A_1 \frac{b_1 x^{c_1}}{1 + b_1 x^{c_1}} \qquad (S1)$$

Where q is the quantity adsorbed(mmol/g), and A_1 is the saturation loadings for adsorption sites A (mmol/g). b_1 represents the constant (kPa^{-c}), and x represents the pressure of bulk gas at equilibrium with adsorbed phase (kPa). The c_1 represents the Freundlich exponent.

1.2 IAST calculations

IAST calculations of C_3H_6/C_3H_8 (50/50, *v*/*v*) adsorption at 298 K were performed by

$$S_{abs} = \frac{q_{C3H6} / q_{C3H8}}{p_{C3H6} / p_{C3H8}} \quad (S2)$$

Similarly, the IAST selectivity for C_2H_4/C_2H_6 (50/50, *v*/*v*) adsorption at 298 K was defined as

$$S_{abs} = \frac{q_{C2H4} / q_{C2H6}}{p_{C2H4} / p_{C2H6}} \quad (S3)$$

where q is the uptake quantities in the mixture, and p is the corresponding mole fraction used in the feed gas mixture.

2 Isosteric heat of adsorption

At 273 K and 298 K ,the Virial equation comprising of the temperature-independent parameters a_i and b_j was employed to calculate the enthalpies of adsorption for C_3H_6 and C_3H_8 in **1** and **1·K**.

$$\ln P = \ln N + {}^{1}/_{k} \sum_{i=0}^{m} a_i N_j + \sum_{j=0}^{n} b_j N_j \quad (S4)$$

Here, P is the pressure expressed in kPa, N is the amount absorbed in mmol g^{-1}, k is the temperature in K, a_i and b_j are Virial coefficients, and m as well as n represent the number of coefficients required to adequately describe the isotherms. The values of the Virial coefficients a_0 through a_m were then used to calculate the isosteric heat of absorption using the following expression:

$$Q_{st} = -R \sum_{i=0}^{m} a_i N_i \quad (S5)$$

Q_{st} represents the coverage-dependent isosteric heat of adsorption (kJ mol^{-1}) and R is the universal gas constant. Based on the adsorption isotherms measured by Micromeritics 3Flexanalyzer, the heat enthalpy of C_3H_6, C_3H_8, C_2H_4 and C_2H_6 for samples were determined at 273 K and 298 K as well as 0-100 kPa.

3 Breakthrough Experiments

Breakthrough experiments for the C_3H_6/C_3H_8 mixtures and C_2H_4/C_2H_6 were performed in a homemade apparatus at 298 K. In the separation experiment, sample **1** (0.88 g for cycle test) and **1·K** (0.631 g for cycle test) samples were packed into a stainless-steel column, followed by activating at 373 K for 12 h under the Helium flow of 20 mL min^{-1}. Then, the adsorption column was dropped to 298 K, followed by introducing the equimolar C_3H_6/C_3H_8 gas mixtures. The raw mixed gas flow rate was maintained at 1 mL min^{-1}. The gas chromatograph monitored the effluent gas by a thermal conductivity detector (TCD).

The C_3H_6 purity (c) is defined by the peak area of C_3H_6, we calculated C_3H_6 purity according to the following equation:

$$c = \frac{C_i(C_3H_6)}{C_i(C_3H_6) + C_i(C_3H_8)} \quad \text{(S6)}$$

where C_i (C_3H_6) and C_i (C_3H_8) represent the peak areas of component C_3H_6 and C_3H_8 in a single injection.

S3 Supplementary figures

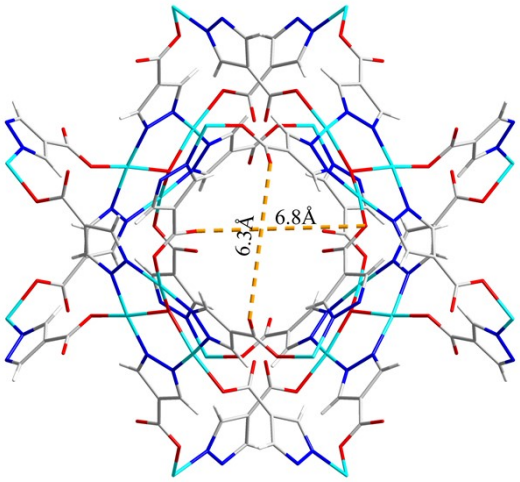

Fig. S1 Partial Enlarged view of the **1** along the crystallographic c-axis.

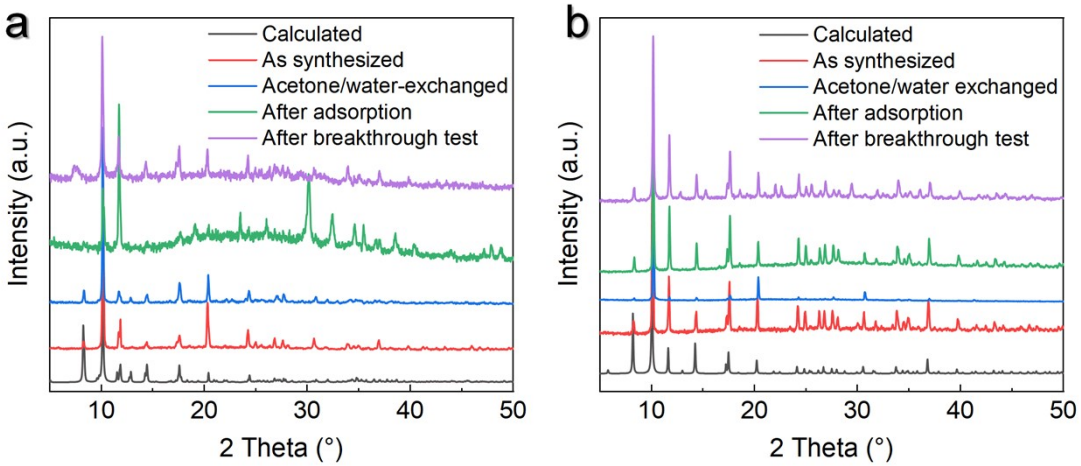

Fig. S2 PXRD patterns for **1** (a) and **1·K** (b) under various conditions.

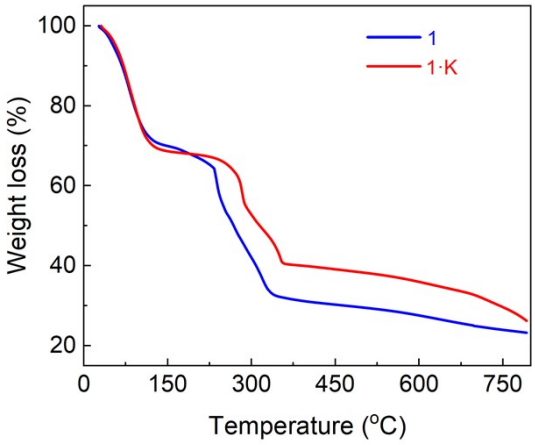

Fig. S3 TGA curves for **1** and **1·K**.

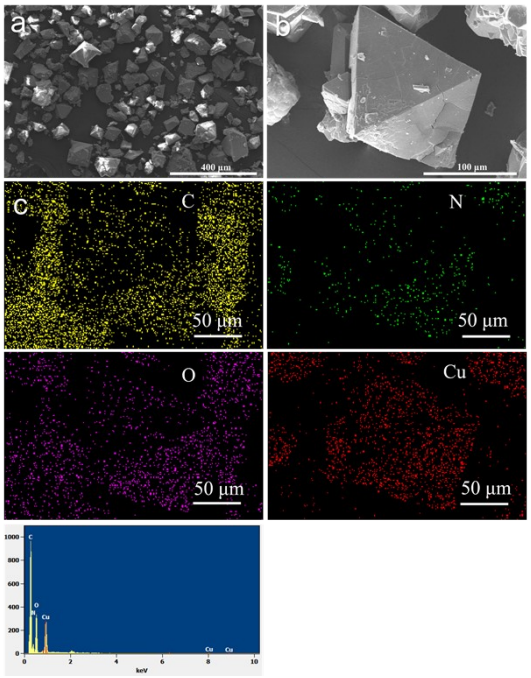

Fig. S4 SEM images (a,b) ,EDS analysis and elemental mapping (c) of **1**.

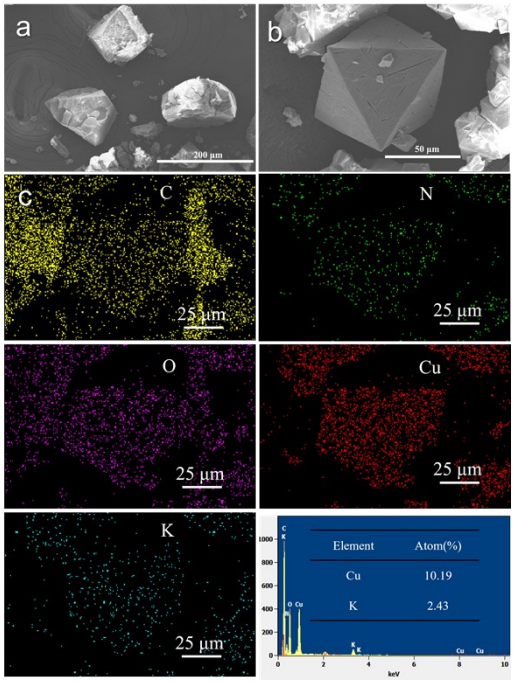

Fig. S5 SEM images (a,b) , EDS analysis and elemental mapping (c) of **1·K**.

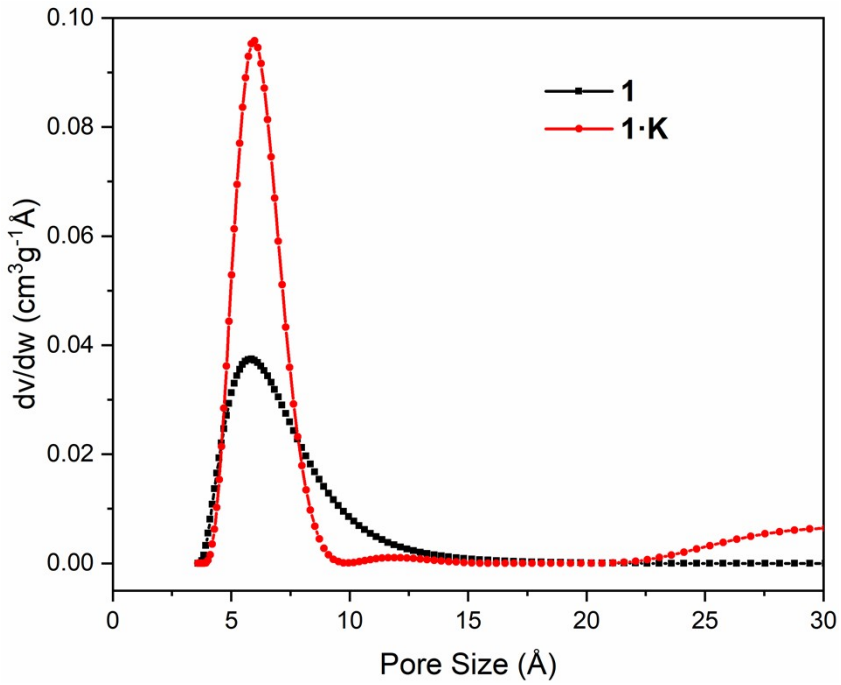

Fig. S6 Pore size distribution for **1** and **1·K** using data measured with N_2 at 77 K.

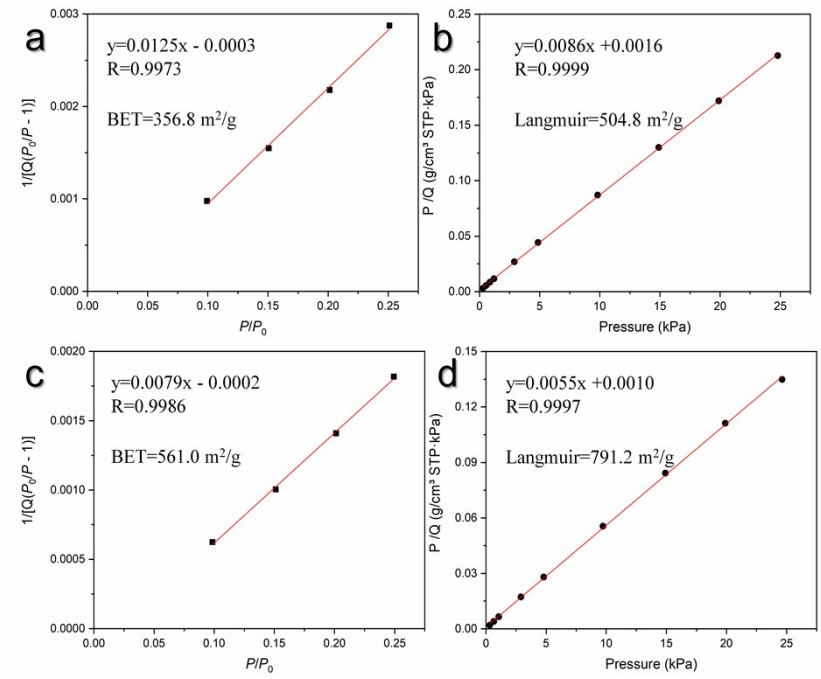

Fig. S7 The BET and Langmuir plots for **1** (a ,b) and **1·K** (c ,d) obtained from the N_2 adsorption isotherm at 77 K.

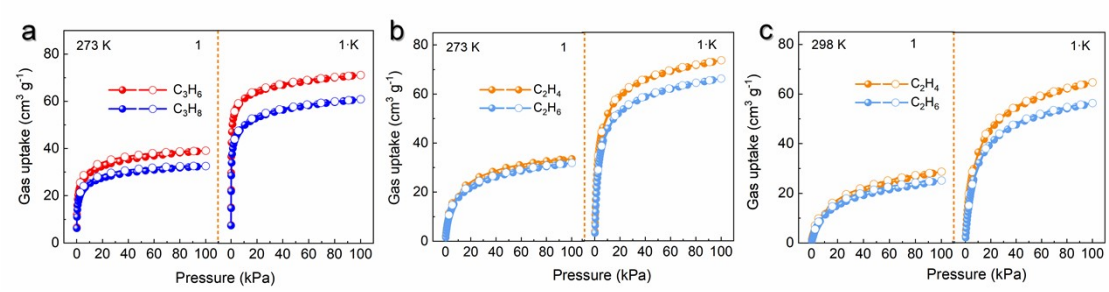

Fig. S8 (a) C_3H_6 and C_3H_8 adsorption isotherms for **1** and **1·K** at 273 K. (b-c) C_2H_4 and C_2H_6 adsorption isotherms for **1** and **1·K** at 273 K and 298 K.

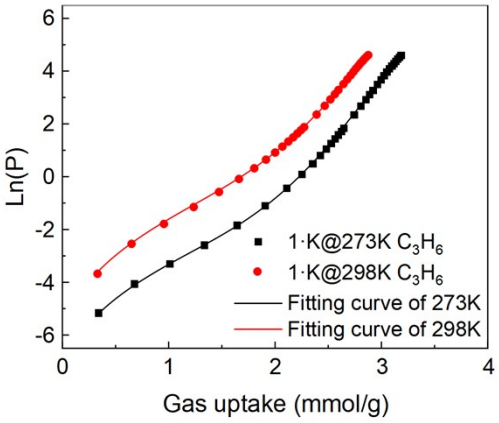

Model	Qst1 (User)	
Equation	ln(x)+1/k*(a0+a1*x+a2*x^2+a3*x^3+a4*x^4+a5*x^5)+(b0+b1*x+b2*x^2)	
Plot	F	H
a0*	-5006.82723 ± 188.01755	-5006.82723 ± 188.01755
a1*	-917.33065 ± 293.91899	-917.33065 ± 293.91899
a2*	664.14862 ± 275.07716	664.14862 ± 275.07716
a3*	-504.13597 ± 171.04172	-504.13597 ± 171.04172
a4*	215.93163 ± 50.82169	215.93163 ± 50.82169
a5*	-28.78876 ± 5.6346	-28.78876 ± 5.6346
b0*	13.98534 ± 0.64021	13.98534 ± 0.64021
b1*	3.57993 ± 0.78841	3.57993 ± 0.78841
b2*	-0.45957 ± 0.21884	-0.45957 ± 0.21884
k	273 ± 0	298 ± 0
Reduced Chi-Sqr*	0.00116	
R-Square (COD)	0.99985	0.99981
R-Square (COD)*	0.99984	
Adj. R-Square*	0.99981	

Fig. S9 Virial fittings (lines) of C_3H_6 adsorption isotherms (symbols) for **1·K** at 273 K and 298 K.

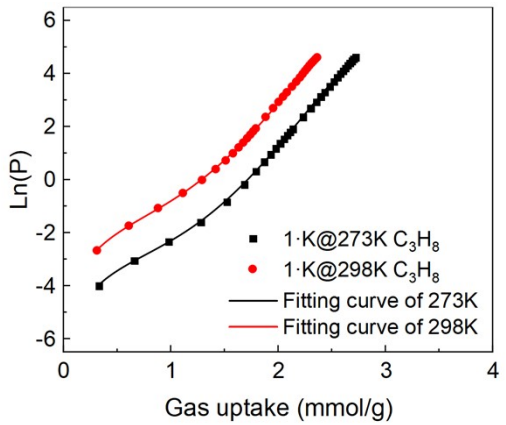

Model	Qst1 (User)	
Equation	ln(x)+1/k*(a0+a1*x+a2*x^2+a3*x^3+a4*x^4+a5*x^5)+(b0+b1*x+b2*x^2)	
Plot	F	H
a0*	-4419.77852 ± 164.7089	-4419.77852 ± 164.7089
a1*	-19.47386 ± 236.0566	-19.47386 ± 236.0566
a2*	-868.52321 ± 103.50125	-868.52321 ± 103.50125
a3*	530.36506 ± 42.62402	530.36506 ± 42.62402
a4*	-96.35574 ± 6.91771	-96.35574 ± 6.91771
a5	0 ± 0	0 ± 0
b0*	12.94902 ± 0.57924	12.94902 ± 0.57924
b1*	1.7916 ± 0.83188	1.7916 ± 0.83188
b2*	0.79854 ± 0.27619	0.79854 ± 0.27619
k	273 ± 0	298 ± 0
Reduced Chi-Sqr*	7.84181E-4	
R-Square (COD)	0.99986	0.99984
R-Square (COD)*	0.99986	
Adj. R-Square*	0.99984	

Fig. S10 Virial fittings (lines) of C_3H_8 adsorption isotherms (symbols) for **1·K** at 273 K and 298 K.

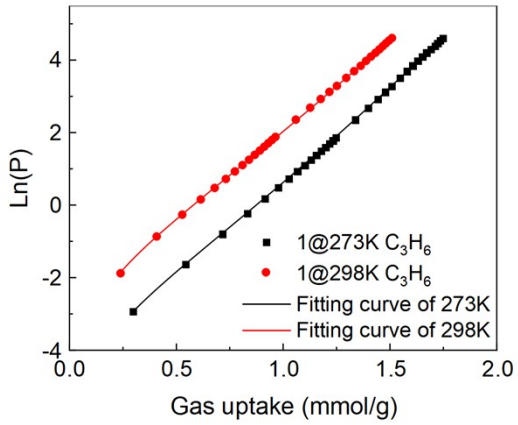

Model	Qst1 (User)	
Equation	ln(x)+1/k*(a0+a1*x+a2*x^2+a3*x^3+a4*x^4+a5*x^5)+(b0+b1*x+b2*x^2)	
Plot	F	H
a0*	-4710.18644 ± 50.68502	-4710.18644 ± 50.68502
a1*	-152.49548 ± 45.75214	-152.49548 ± 45.75214
a2*	319.19763 ± 29.28074	319.19763 ± 29.28074
a3*	-25.91119 ± 9.55016	-25.91119 ± 9.55016
a4	0 ± 0	0 ± 0
a5	0 ± 0	0 ± 0
b0*	14.84699 ± 0.17835	14.84699 ± 0.17835
b1*	2.51783 ± 0.15345	2.51783 ± 0.15345
b2	0 ± 0	0 ± 0
k	273 ± 0	298 ± 0
Reduced Chi-Sqr*	2.61516E-4	
R-Square (COD)	0.99993	0.99992
R-Square (COD)*	0.99993	
Adj. R-Square*	0.99992	

Fig. S11 Virial fittings (lines) of C_3H_6 adsorption isotherms (symbols) for **1** at 273 K and 298 K.

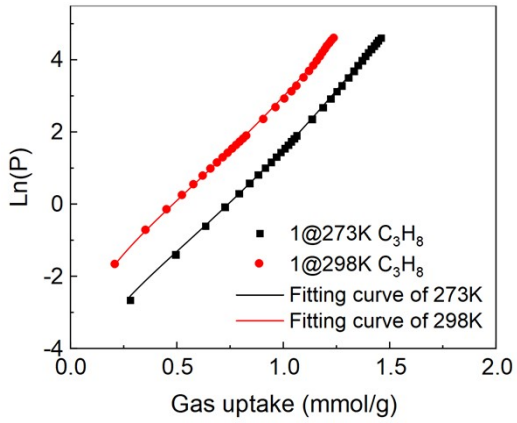

Model	Qst1 (User)	
Equation	ln(x)+1/k*(a0+a1*x+a2*x^2+a3*x^3+a4*x^4+a5*x^5)+(b0+b1*x+b2*x^2)	
Plot	F	H
a0*	-4184.2734 ± 137.67625	-4184.2734 ± 137.67625
a1*	-1033.73578 ± 150.04678	-1033.73578 ± 150.04678
a2*	443.33473 ± 111.85284	443.33473 ± 111.85284
a3*	20.30381 ± 43.28763	20.30381 ± 43.28763
a4	0 ± 0	0 ± 0
a5	0 ± 0	0 ± 0
b0*	13.4409 ± 0.48123	13.4409 ± 0.48123
b1*	5.49181 ± 0.49433	5.49181 ± 0.49433
b2	0 ± 0	0 ± 0
k	273 ± 0	298 ± 0
Reduced Chi-Sqr*	0.0017	
R-Square (COD)	0.99984	0.99908
R-Square (COD)*	0.9995	
Adj. R-Square*	0.99946	

Fig. S12 Virial fittings (lines) of C_3H_8 adsorption isotherms (symbols) for **1** at 273 K and 298 K.

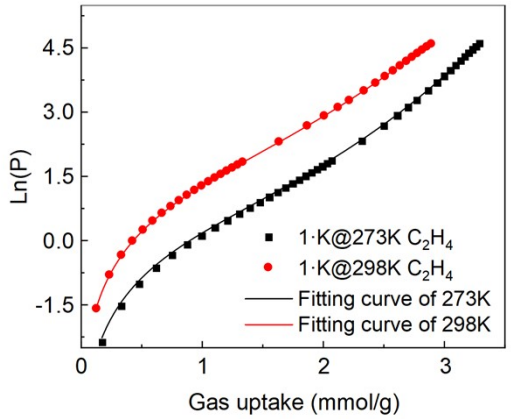

Model	Qst1 (User)	
Equation	ln(x)+1/k*(a0+a1*x+a2*x^2+a3*x^3+a4*x^4+a5*x^5)+(b0+b1*x+b2*x^2)	
Plot	F	H
a0*	-3498.70867 ± 85.49463	-3498.70867 ± 85.49463
a1*	81.40875 ± 135.58641	81.40875 ± 135.58641
a2*	-331.96602 ± 97.69685	-331.96602 ± 97.69685
a3*	205.09702 ± 61.91304	205.09702 ± 61.91304
a4*	-49.11264 ± 19.55163	-49.11264 ± 19.55163
a5*	5.01237 ± 2.26141	5.01237 ± 2.26141
b0*	12.06362 ± 0.29264	12.06362 ± 0.29264
b1*	1.32431 ± 0.41618	1.32431 ± 0.41618
b2*	-0.06544 ± 0.12504	-0.06544 ± 0.12504
k	273 ± 0	298 ± 0
Reduced Chi-Sqr*	7.25149E-4	
R-Square (COD)	0.9998	0.99978
R-Square (COD)*	0.99979	
Adj. R-Square*	0.99977	

Fig. S13 Virial fittings (lines) of C_2H_4 adsorption isotherms (symbols) for **1·K** at 273 K and 298 K.

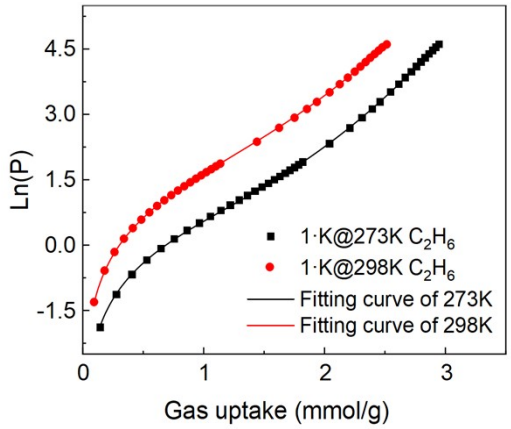

Model	Qst1 (User)	
Equation	ln(x)+1/k*(a0+a1*x+a2*x^2+a3*x^3+a4*x^4+a5*x^5)+(b0+b1*x+b2*x^2)	
Plot	F	H
a0*	-3187.46905 ± 24.4918	-3187.46905 ± 24.4918
a1*	-322.49482 ± 21.21173	-322.49482 ± 21.21173
a2*	-137.07742 ± 17.37189	-137.07742 ± 17.37189
a3*	90.07978 ± 8.46227	90.07978 ± 8.46227
a4*	-10.16046 ± 1.38117	-10.16046 ± 1.38117
a5	0 ± 0	0 ± 0
b0*	11.65804 ± 0.08418	11.65804 ± 0.08418
b1*	1.95396 ± 0.05251	1.95396 ± 0.05251
b2	0 ± 0	0 ± 0
k	273 ± 0	298 ± 0
Reduced Chi-Sqr*	1.82104E-4	
R-Square (COD)	0.99995	0.99993
R-Square (COD)*	0.99994	
Adj. R-Square*	0.99994	

Fig. S14 Virial fittings (lines) of C_2H_6 adsorption isotherms (symbols) for **1·K** at 273 K and 298 K.

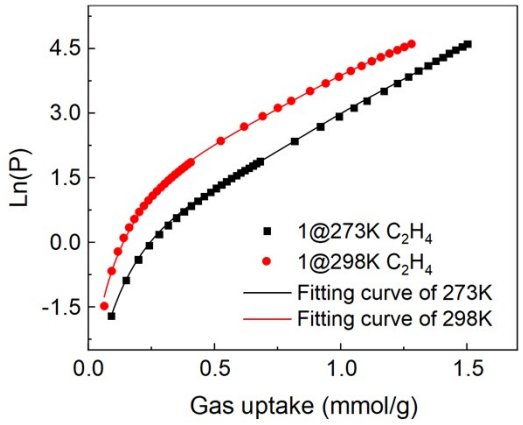

Model	Qst1 (User)	
Equation	ln(x)+1/k*(a0+a1*x+a2*x^2+a3*x^3+a4*x^4+a5*x^5)+(b0+b1*x+b2*x^2)	
Plot	F	H
a0*	-3347.62801 ± 115.03469	-3347.62801 ± 115.03469
a1*	1169.34683 ± 457.70152	1169.34683 ± 457.70152
a2*	-5428.47011 ± 713.62248	-5428.47011 ± 713.62248
a3*	8814.90521 ± 953.74172	8814.90521 ± 953.74172
a4*	-5272.48246 ± 676.33617	-5272.48246 ± 676.33617
a5*	1189.17574 ± 174.94348	1189.17574 ± 174.94348
b0*	12.17158 ± 0.38832	12.17158 ± 0.38832
b1*	6.20626 ± 1.37207	6.20626 ± 1.37207
b2*	-4.85943 ± 0.95583	-4.85943 ± 0.95583
k	273 ± 0	298 ± 0
Reduced Chi-Sqr*	0.00147	
R-Square (COD)	0.99983	0.99916
R-Square (COD)*	0.99951	
Adj. R-Square*	0.99945	

Fig. S15 Virial fittings (lines) of C_2H_4 adsorption isotherms (symbols) for **1** at 273 K and 298 K.

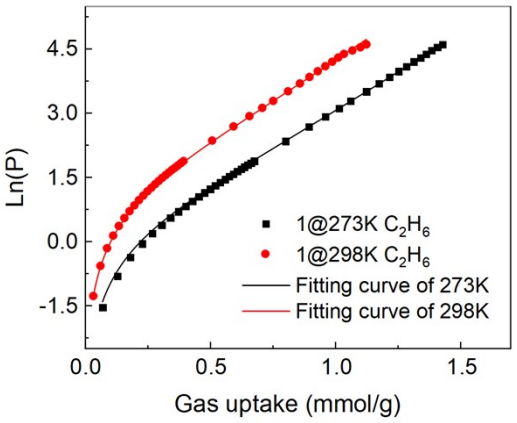

Model	Qst1 (User)	
Equation	ln(x)+1/k*(a0+a1*x+a2*x^2+a3*x^3+a4*x^4+a5*x^5)+(b0+b1*x+b2*x^2)	
Plot	F	H
a0*	-3085.77702 ± 111.73547	-3085.77702 ± 111.73547
a1*	-297.09327 ± 470.2921	-297.09327 ± 470.2921
a2*	-1028.20845 ± 692.27009	-1028.20845 ± 692.27009
a3*	1170.28112 ± 972.27269	1170.28112 ± 972.27269
a4*	-798.92594 ± 745.21536	-798.92594 ± 745.21536
a5*	200.99242 ± 206.50513	200.99242 ± 206.50513
b0*	12.45473 ± 0.37902	12.45473 ± 0.37902
b1*	2.98782 ± 1.47571	2.98782 ± 1.47571
b2*	1.67943 ± 1.17102	1.67943 ± 1.17102
k	273 ± 0	298 ± 0
Reduced Chi-Sqr*	0.00143	
R-Square (COD)	0.99949	0.99951
R-Square (COD)*	0.9995	
Adj. R-Square*	0.99944	

Fig. S16 Virial fittings (lines) of C_2H_6 adsorption isotherms (symbols) for **1** at 273 K and 298 K.

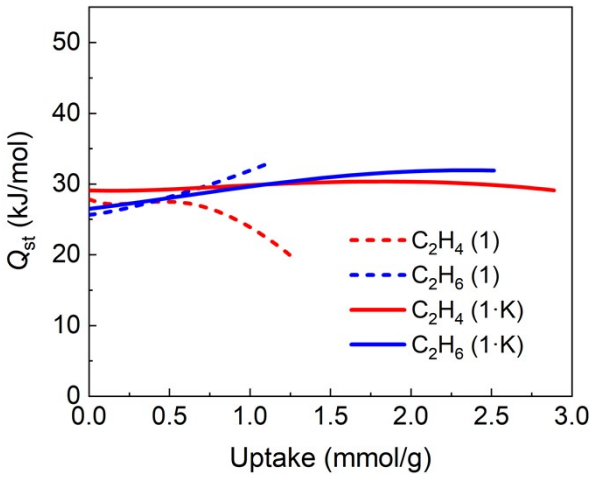

Fig. S17 Comparison of Q_{st} of **1** and **1·K** for C_2H_4 and C_2H_6.

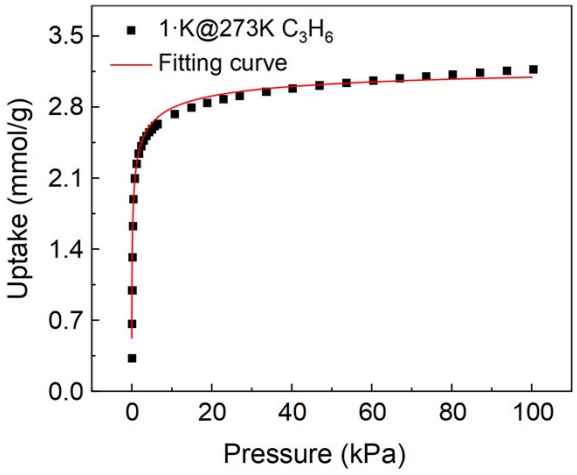

Model	LFUser (User)
Equation	A1*b1*x^c1/(1+b1*x^c1)
Plot	B
A1	3.28829 ± 0.04722
b1	1.95531 ± 0.12733
c1	0.45531 ± 0.02034
Reduced Chi-Sqr	0.00464
R-Square (COD)	0.99222
Adj. R-Square	0.99168

Fig. S18 Single-site Langmuir-Freundlich (L-F) model fitting for C_3H_6 isotherm of **1·K** at 273 K.

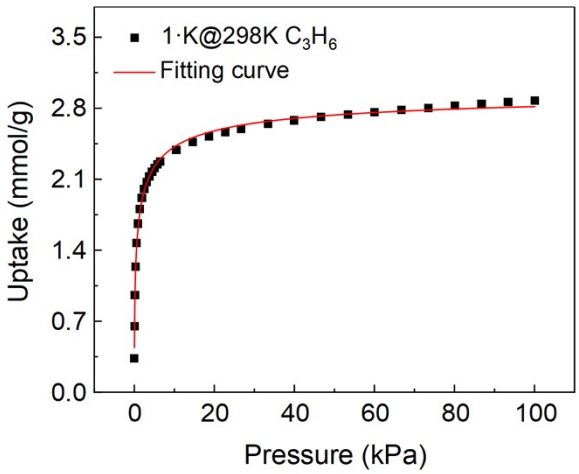

Model	LFUser (User)
Equation	A1*b1*x^c1/(1+b1*x^c1)
Plot	D
A1	3.02635 ± 0.03274
b1	1.18126 ± 0.03951
c1	0.52743 ± 0.01662
Reduced Chi-Sqr	0.00174
R-Square (COD)	0.99644
Adj. R-Square	0.99618

Fig. S19 Single-site Langmuir-Freundlich (L-F) model fitting for C_3H_6 isotherm of **1·K** at 298 K.

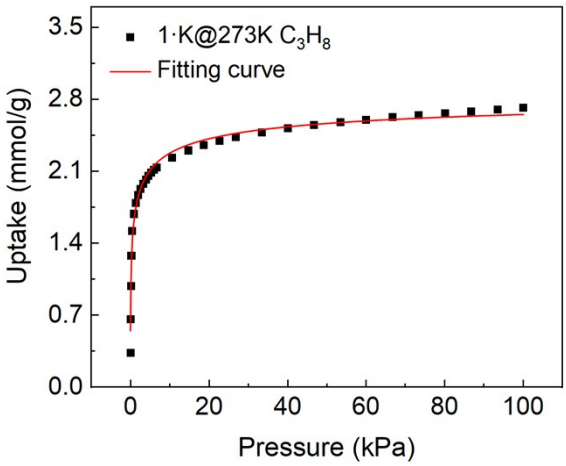

Model	LFUser (User)
Equation	A1*b1*x^c1/(1+b1*x^c1)
Plot	B
A1	2.93874 ± 0.07316
b1	1.27308 ± 0.09588
c1	0.42987 ± 0.02642
Reduced Chi-Sqr	0.00497
R-Square (COD)	0.9875
Adj. R-Square	0.98661

Fig. S20 Single-site Langmuir-Freundlich (L-F) model fitting for C_3H_8 isotherm of **1·K** at 273 K.

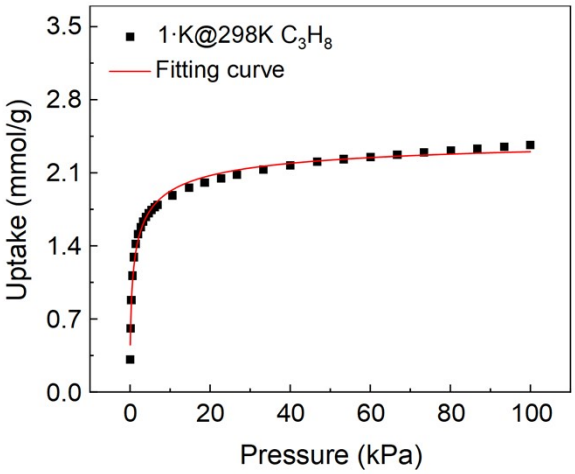

Model	LFUser (User)
Equation	A1*b1*x^c1/(1+b1*x^c1)
Plot	D
A1	2.49693 ± 0.04565
b1	0.95158 ± 0.04437
c1	0.5467 ± 0.02799
Reduced Chi-Sqr	0.00263
R-Square (COD)	0.9913
Adj. R-Square	0.99065

Fig. S21 Single-site Langmuir-Freundlich (L-F) model fitting for C_3H_8 isotherm of **1·K** at 298 K.

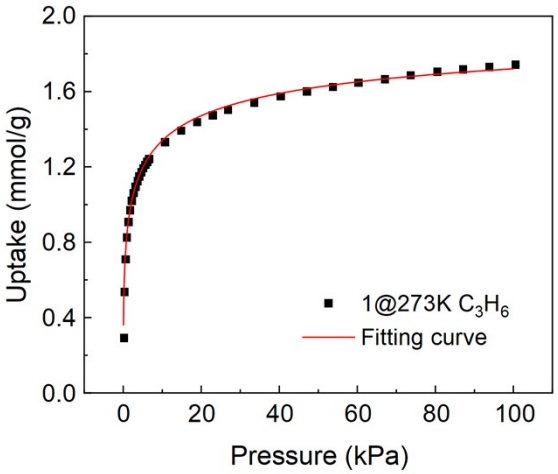

Model	LFUser (User)
Equation	A1*b1*x^c1/(1+b1*x^c1)
Plot	B
A1	2.10059 ± 0.0383
b1	0.68378 ± 0.02111
c1	0.41054 ± 0.01291
Reduced Chi-Sqr	3.38283E-4
R-Square (COD)	0.99768
Adj. R-Square	0.99752

Fig. S22 Single-site Langmuir-Freundlich (L-F) model fitting for C_3H_6 isotherm of **1** at 273 K.

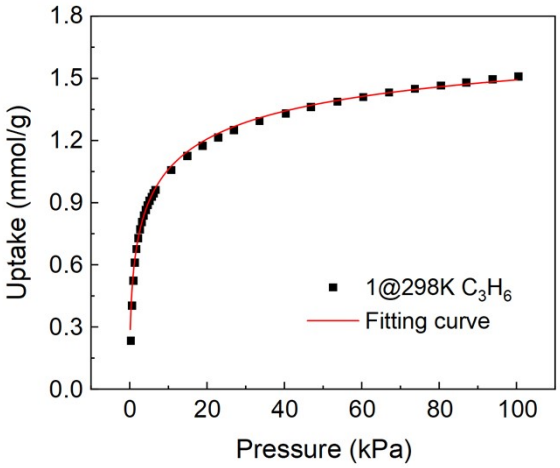

Model	LFUser (User)
Equation	A1*b1*x^c1/(1+b1*x^c1)
Plot	D
A1	1.88818 ± 0.03832
b1	0.43437 ± 0.01106
c1	0.46937 ± 0.01383
Reduced Chi-Sqr	2.19789E-4
R-Square (COD)	0.99834
Adj. R-Square	0.99822

Fig. S23 Single-site Langmuir-Freundlich (L-F) model fitting for C_3H_6 isotherm of **1** at 298 K.

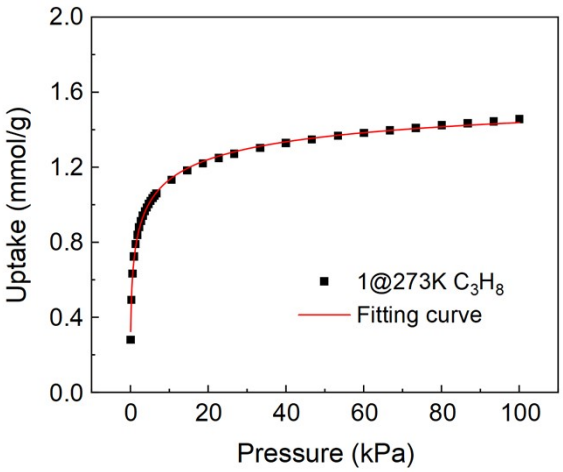

Model	LFUser (User)
Equation	A1*b1*x^c1/(1+b1*x^c1)
Plot	B
A1	1.7088 ± 0.02225
b1	0.73019 ± 0.01657
c1	0.43056 ± 0.01079
Reduced Chi-Sqr	1.52131E-4
R-Square (COD)	0.9984
Adj. R-Square	0.99829

Fig. S24 Single-site Langmuir-Freundlich (L-F) model fitting for C_3H_8 isotherm of **1** at 273 K.

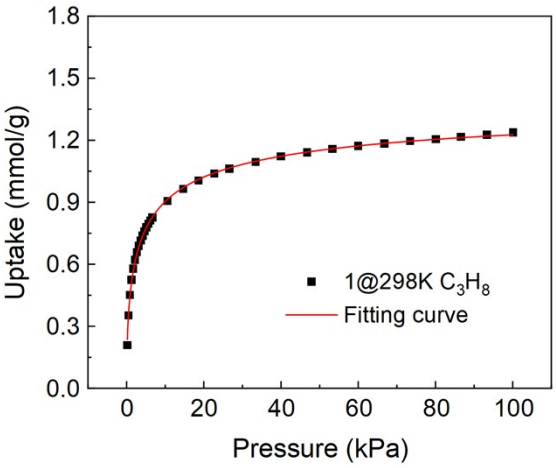

Model	LFUser (User)
Equation	A1*b1*x^c1/(1+b1*x^c1)
Plot	D
A1	1.42986 ± 0.01183
b1	0.48853 ± 0.00545
c1	0.54551 ± 0.00879
Reduced Chi-Sqr	5.42528E-5
R-Square (COD)	0.99938
Adj. R-Square	0.99933

Fig. S25 Single-site Langmuir-Freundlich (L-F) model fitting for C_3H_8 isotherm of **1** at 298 K.

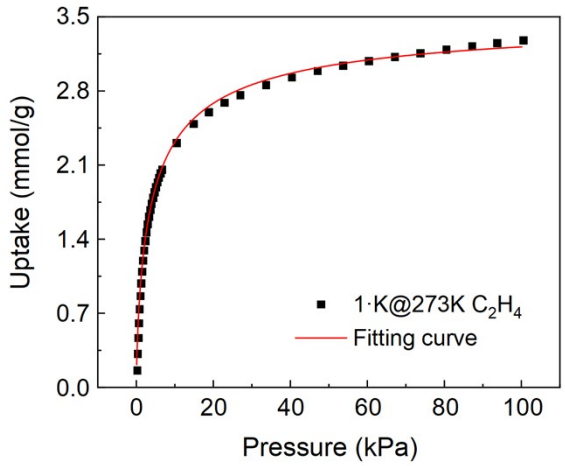

Model	LFUser (User)
Equation	A1*b1*x^c1/(1+b1*x^c1)
Plot	B
A1	3.53072 ± 0.02869
b1	0.3575 ± 0.00471
c1	0.72825 ± 0.01304
Reduced Chi-Sqr	0.00103
R-Square (COD)	0.99887
Adj. R-Square	0.99881

Fig. S26 Single-site Langmuir-Freundlich (L-F) model fitting for C_2H_4 isotherm of **1·K** at 273 K.

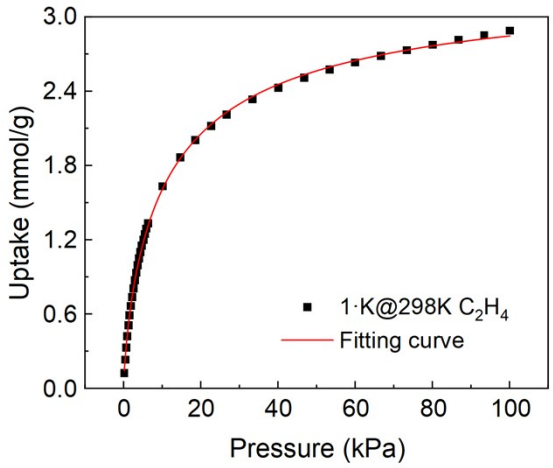

Model	LFUser (User)
Equation	A1*b1*x^c1/(1+b1*x^c1)
Plot	D
A1	3.36107 ± 0.02946
b1	0.15083 ± 0.00159
c1	0.78199 ± 0.01007
Reduced Chi-Sqr	3.42477E-4
R-Square (COD)	0.9996
Adj. R-Square	0.99958

Fig. S27 Single-site Langmuir-Freundlich (L-F) model fitting for C_2H_4 isotherm of **1·K** at 298 K.

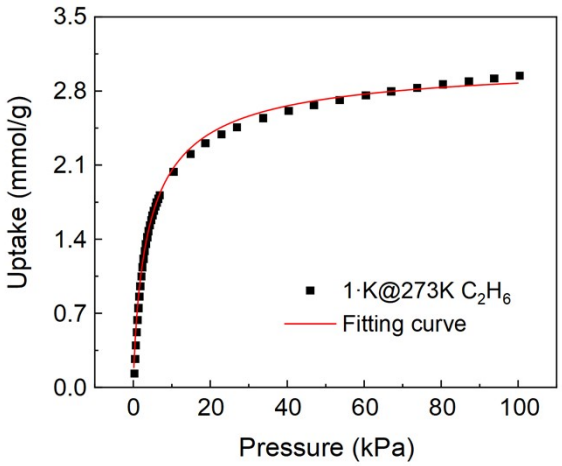

Model	LFUser User)
Equation	A1*b1*x^c1/(1+b1*x^c1)
Plot	B
A1	3.10265 ± 0.02924
b1	0.30019 ± 0.00543
c1	0.81192 ± 0.01836
Reduced Chi-Sqr	0.00138
R-Square (COD)	0.99814
Adj. R-Square	0.99804

Fig. S28 Single-site Langmuir-Freundlich (L-F) model fitting for C_2H_6 isotherm of **1·K** at 273 K.

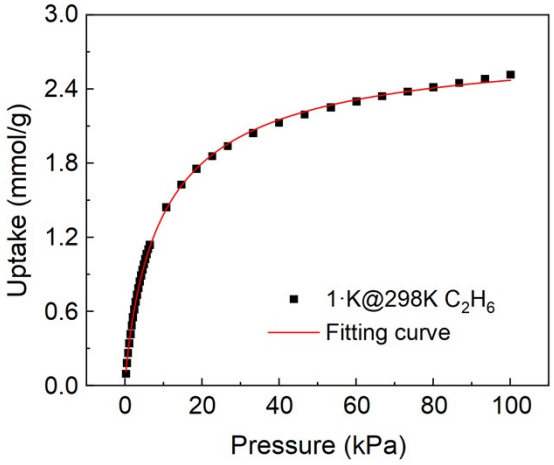

Model	LFUser (User)
Equation	A1*b1*x^c1/(1+b1*x^c1)
Plot	D
A1	2.81076 ± 0.02288
b1	0.12928 ± 0.00174
c1	0.87445 ± 0.01199
Reduced Chi-Sqr	3.25436E-4
R-Square (COD)	0.99952
Adj. R-Square	0.99949

Fig. S29 Single-site Langmuir-Freundlich (L-F) model fitting for C_2H_6 isotherm of **1·K** at 298 K.

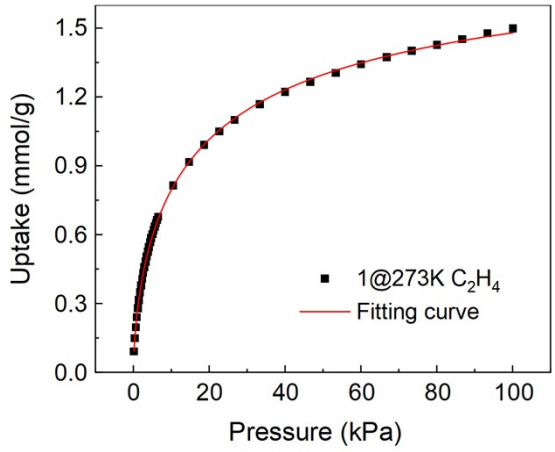

Model	LFUser (User)
Equation	A1*b1*x^c1/(1+b1*x^c1)
Plot	B
A1	1.96144 ± 0.02146
b1	0.15105 ± 0.00134
c1	0.65409 ± 0.00734
Reduced Chi-Sqr	5.87269E-5
R-Square (COD)	0.99971
Adj. R-Square	0.99969

Fig. S30 Single-site Langmuir-Freundlich (L-F) model fitting for C_2H_4 isotherm of **1** at 273 K.

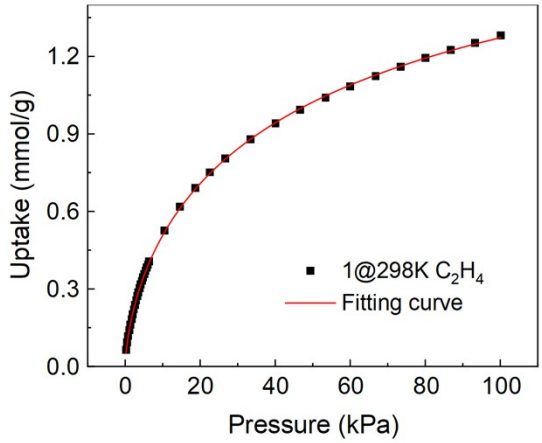

Model	LFUser (User)
Equation	A1*b1*x^c1/(1+b1*x^c1)
Plot	D
A1	2.18406 ± 0.03134
b1	0.06558 ± 6.96526E-4
c1	0.664 ± 0.00511
Reduced Chi-Sqr	1.90573E-5
R-Square (COD)	0.99989
Adj. R-Square	0.99988

Fig. S31 Single-site Langmuir-Freundlich (L-F) model fitting for C_2H_4 isotherm of **1** at 298 K.

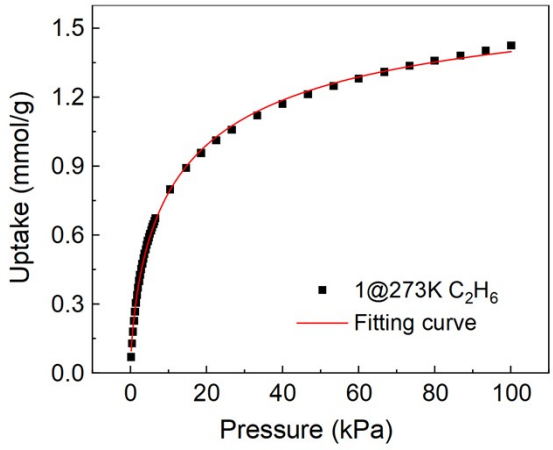

Model	LFUser (User)
Equation	A1*b1*x^c1/(1+b1*x^c1)
Plot	B
A1	1.75199 ± 0.02883
b1	0.16565 ± 0.00237
c1	0.6883 ± 0.01376
Reduced Chi-Sqr	1.81776E-4
R-Square (COD)	0.99897
Adj. R-Square	0.99891

Fig. S32 Single-site Langmuir-Freundlich (L-F) model fitting for C_2H_6 isotherm of **1** at 273 K.

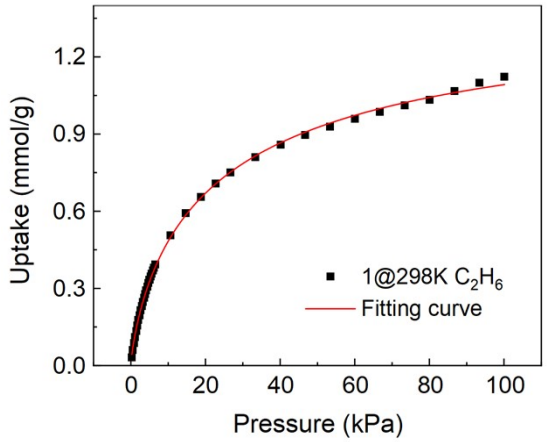

Model	LFUser (User)
Equation	A1*b1*x^c1/(1+b1*x^c1)
Plot	D
A1	1.46015 ± 0.03026
b1	0.08246 ± 0.0014
c1	0.77807 ± 0.01489
Reduced Chi-Sqr	1.11616E-4
R-Square (COD)	0.99913
Adj. R-Square	0.99908

Fig. S33 Single-site Langmuir-Freundlich (L-F) model fitting for C_2H_6 isotherm of **1** at 298 K.

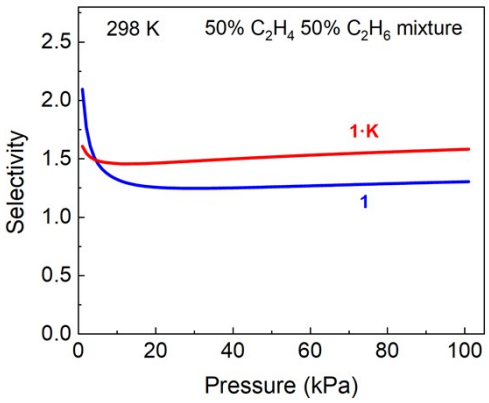

Fig. S34 IAST selectivities of **1** and **1·K** for equimolar C_2H_4/C_2H_6 at 298 K.

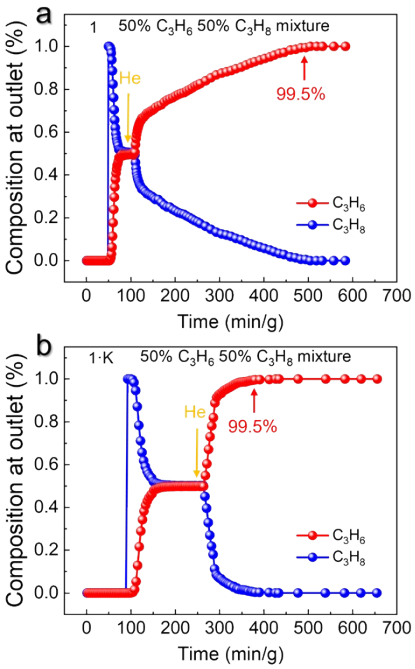

Fig. S35 Outlet C_3H_6 (red) and C_3H_8 (blue) compositions of the adsorption-desorption cycle in the breakthrough experiment for **1** (a) and **1·K** (b)

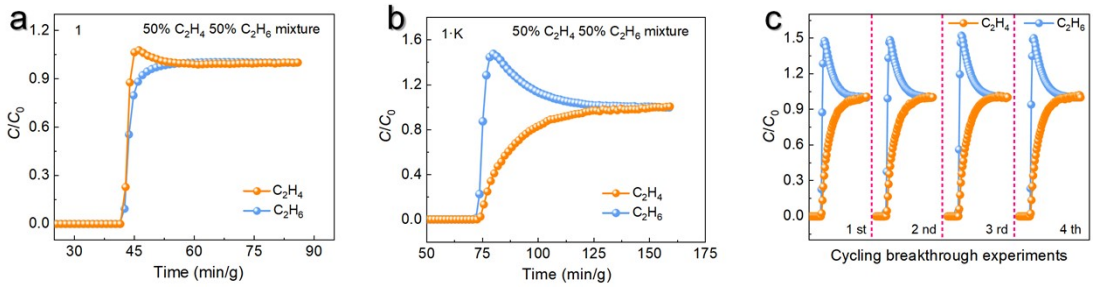

Fig. S36 The single dynamic breakthrough curves of **1** (a) and **1·K** (b) with equimolar C_2H_4/C_2H_6 gas mixtures at 298 K and 100 kPa. (c) Cycling stability of **1·K**.

S4 Supplementary tables

Table S1 ICP analysis results of **1·K**.

Sample	K (μg/mL)	Cu (μg/mL)	Zn (μg/mL)	Cu : K (% at. / % at.)
1·K	2.62	13.1	/	3:1

Table S2 Summary of the adsorption capacity of C_3H_6 and C_3H_8 and C_3H_6/C_3H_8 (50/50) selectivity in some MOFs.

No	**MOFs**	**C_3H_6 uptake ($cm^3\ g^{-1}$)**	**C_3H_8 uptake ($cm^3\ g^{-1}$)**	**IAST selectivity (50/50)**	**Conditions**	**Refs**
1	CuBTC	179.20	152.32	/	323K, 100kPa	1
2	KAUST-7	32.00	1.20	/	298K, 100kPa	2
3	Zn_2(dobdc)	140.90	122.30	3.89	318K, 100kPa	3
4	Mg_2(dobdc)	167.10	134.40	5.55	318K, 100kPa	3
5	NJU-Bai8	60.48	1.34	4.60	298K, 20kPa	4
6	GeFSIX-2-Cu-i	60.26	40.54	4.00	298K, 100kPa	5

7	SiFSIX-2-Cu-i	59.36	37.41	4.50	298K, 100kPa	[5]
8	Ni-NP	79.97	47.71	10.5	298K, 100kPa	[6]
9	MAF-23-O	30.2	22.4	8.80	298K, 100kPa	[7]
10	HIAM-301	70.784	0.67	150	298K, 100kPa	[8]
11	JNU-3a	58.60	48.0	513	303K, 100kPa	[9]
12	NTU-85-WNT	10.15	0.06	1570.3	298K, 100kPa	[10]
13	**1**	33.8	27.7	2.20	298K, 100kPa	This work
14	**1·K**	64.5	53.0	4.38	298K, 100kPa	This work

References

1 N. Lamia, M. Jorge, M. A. Granato, F. A. Almeida Paz, H. Chevreau and A. E. Rodrigues, Chem. Eng. Sci., 2009, **64**, 3246-3259.

2 A. Cadiau, K. Adil, P. M. Bhatt, Y. Belmabkhout and M. Eddaoudi,*Science*, 2016, **353**, 137-140.

3 S. J. Geier, J. A. Mason, E. D. Bloch, W. L. Queen, M. R. Hudson, C. M. Brown and J. R. Long, *Chem. Sci*., 2013, **4**, 2054-2061.

4 X. Wang, R. Krishna, L. Li, B. Wang, T. He, Y.-Z. Zhang, J.-R. Li and J. Li, *Chem*. *Eng*. *J*., 2018, **346**, 489-496.

5 X. Wang, P. Zhang, Z. Zhang, L. Yang, Q. Ding, X. Cui, J. Wang and H. Xing, *Ind. Eng*. *Chem*. *Res*., 2020, **59**, 3531-3537.

6 Y. Xie, Y. Shi, H. Cui, R.-B. Lin and B. Chen, *Small Struct*., 2022, **3**, 2100125.

7 Y. Wang, N. Y. Huang, X. W. Zhang, H. He, R. K. Huang, Z. M. Ye, Y. Li, D. D. Zhou, P. Q. Liao, X. M. Chen and J. P. Zhang, *Angew*. *Chem*. *Int*. *Ed*., 2019, **58**, 7692-7696.

8 L. Yu, X. Han, H. Wang, S. Ullah, Q. Xia, W. Li, J. Li, I. da Silva, P. Manuel, S. Rudic, Y. Cheng, S. Yang, T. Thonhauser and J. Li, *J*. *Am*. *Chem*. *Soc*., 2021, **143**, 19300-19305.

9 H. Zeng, M. Xie, T. Wang, R. J. Wei, X. J. Xie, Y. Zhao, W. Lu and D. Li, *Nature*, 2021, **595**, 542-548.

10 Q. Dong, Y. Huang, J. Wan, Z. Lu, Z. Wang, C. Gu, J. Duan and J. Bai, *J*. *Am*. *Chem*. *Soc*., 2023, **145**, 8043-8051.